

Molecular Modeling Study of the SO₂ Deactivation of an Amine Resin and a Procedure to Avoid SO₂ Deactivation Using a Polyethylene Glycol/Tertiary Amine System

Buijs, Wim

DOI

[10.1021/acs.iecr.0c01800](https://doi.org/10.1021/acs.iecr.0c01800)

Publication date

2020

Document Version

Final published version

Published in

Industrial and Engineering Chemistry Research

Citation (APA)

Buijs, W. (2020). Molecular Modeling Study of the SO₂ Deactivation of an Amine Resin and a Procedure to Avoid SO₂ Deactivation Using a Polyethylene Glycol/Tertiary Amine System. *Industrial and Engineering Chemistry Research*, 59(30), 13388-13395. <https://doi.org/10.1021/acs.iecr.0c01800>

Important note

To cite this publication, please use the final published version (if applicable). Please check the document version above.

Copyright

Other than for strictly personal use, it is not permitted to download, forward or distribute the text or part of it, without the consent of the author(s) and/or copyright holder(s), unless the work is under an open content license such as Creative Commons.

Takedown policy

Please contact us and provide details if you believe this document breaches copyrights. We will remove access to the work immediately and investigate your claim.

Molecular Modeling Study of the SO₂ Deactivation of an Amine Resin and a Procedure To Avoid SO₂ Deactivation Using a Polyethylene Glycol/Tertiary Amine System

Wim Buijs*

Cite This: *Ind. Eng. Chem. Res.* 2020, 59, 13388–13395

Read Online

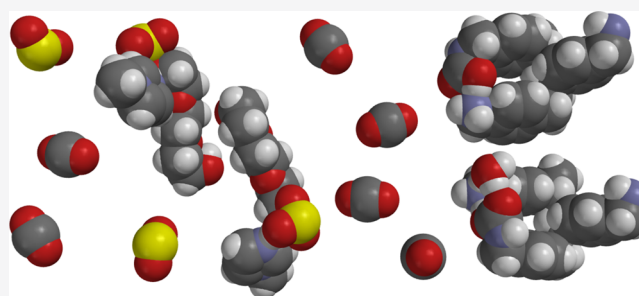
ACCESS |

Metrics & More

Article Recommendations

Supporting Information

ABSTRACT: Since 2012, the polymeric resin Lewatit R VP OC 1065 has been investigated for removal of CO₂ from various process streams and air. The present article focuses on the deactivation mechanism of the resin with SO₂ and a work around. This is important for CO₂ capture from flue gas of coal-fired power plants and fuel oil. The deactivation of the resin was already experimentally observed in 2013 but thus far not described computationally. Molecular modeling shows that Lewatit R VP OC 1065 is deactivated by irreversible formation of dimeric amine–SO₂ charge-transfer complexes which are very stable and resist thermal and chemical desorption. Additional support for this view was found in the work on aminosilica adsorbents for CO₂ capture, which are subject to SO₂ deactivation also. Therefore, attention was paid to a procedure to avoid SO₂ deactivation. Polyethylene glycol (PEG)/tertiary amine systems seem to be very promising. Their reported high SO₂/CO₂ selectivities, SO₂ capacities, and ease of regeneration were computationally confirmed by identifying their mode of action and favorable thermodynamics. As a result, a combination of a PEG/tertiary amine system with Lewatit R VP OC 1065 might be a very attractive candidate two-step process to capture both SO₂ and CO₂ from flue gas originating from coal-fired power plants and large ships.



INTRODUCTION

In the last decade, the discussion on the contribution of anthropogenic CO₂ emissions to the increase of the CO₂ level in the atmosphere and global warming has settled,^{1,2} and nowadays, it is almost accepted worldwide that CO₂ capture for sequestration, storage, or utilization is a necessity to reduce the increasingly visible negative effects of global warming.

Already in 2012, a favorable material for CO₂ capture but not for storage(!) was described.³ The polymeric resin Lewatit R VP OC 1065 showed good capacity for CO₂ adsorption and desorption under various process conditions ranging from CO₂-rich flue gas (>10% CO₂) to even the atmospheric CO₂ level of approximately 400 ppm. Possibly, even more important was its low H₂O-uptake (1.5 mol/kg resin) as a high H₂O adsorption and desorption would otherwise dominate the energy consumption of the overall process and block most if not all practical applications. However, the same research group reported in 2013, complete deactivation by O₂ at 120 °C in air and SO₂ at 431 ppm at ambient temperature.^{4,5} In 2017, Yu et al.⁶ confirmed oxidative degradation above 70 °C in air and also degradation in concentrated dry CO₂ above 120 °C; however, they did not investigate SO₂ deactivation. In a computational study from 2017, a structural model for Lewatit R VP OC 1065 was developed and the CO₂ capturing reactions were described quantitatively.⁷ As the focus of the research on Lewatit R VP OC

1065 was directed toward Direct Air Capture of CO₂, in 2019, the deactivation reactions by CO₂ and O₂ were described too, including operational strategies to avoid deactivation by CO₂ and O₂.^{8,9} However, deactivation of the Lewatit resin by SO₂ was not investigated further neither experimentally nor computationally until now. Rezaei and Jones^{10,11} reported SO₂ deactivation on aminosilica adsorbents for CO₂ capture in a systematic experimental study using primary, secondary, and tertiary amines, and polyethylene imine silica materials containing a mixture of primary, secondary, and tertiary amine groups.

Between 1980 and 2018, a 93% decrease in the SO₂ level in air to ~20 ppb was observed in the USA¹² and in Europe¹³ because of the extensive desulfurization programs; however, still occasionally peak levels of 400–700 ppb¹⁴ are observed. Where an average level of 20 ppb SO₂ and 400 ppm CO₂ would lead to a life-time expectancy of the resin of 20,000 cycles (>5 years), a peak level of 700 ppb for ~1 day/month leads to a

Received: April 9, 2020
Revised: June 3, 2020
Accepted: June 18, 2020
Published: June 18, 2020



complete loss of CO₂ capacity of the resin in 1 year. Furthermore, both CO₂ and SO₂ emissions from ships using fuel oil are considerable. The average sulfur content of fuel oil is 2.7%; however, since 2012, the maximum allowed level is 0.5%.¹⁵ This S-level is way too high to allow CO₂ capture from the flue gas of large ships. Finally, there are still a lot of coal-fired power stations in place, which could diminish their carbon footprint by SO₂ and CO₂ capture. Therefore, it is still necessary to identify the deactivation mechanism by SO₂ and to develop a procedure to avoid SO₂ deactivation of this particular resin.

MOLECULAR MODELING

All molecular modeling studies were performed using Wavefunction's Spartan'18 suite.¹⁶ Molecular mechanics (MMFF) was used to explore the physisorption complexes of SO₂ with the saturated trimer of 4-aminomethyl vinyl benzene,⁷ a previously obtained model for Lewatit R VP OC 1065, *n*-propyl amine, *N*-methyl propyl amine, and *N,N*-dimethyl propyl amine, and the linear trimer of ethylene glycol, a model for polyethylene glycol (PEG), *N*-methyl imidazole, and *N*-methyl⁺ diazo bicycle octane Br⁻. MMFF results were used as starting structures for calculations wherein physisorption and particularly chemical reactions were investigated further, using density functional theory B3LYP/6-31-G* as reported earlier.⁷ Quantitative results of all calculations and all molecular (ensemble) structures are available in [Supporting Information](#).

RESULTS AND DISCUSSION

Calibration of the computational results with the experimental data is crucial in order to obtain reliable conclusions. Two aspects are important in the calibration: structural and energetic accuracy. Sulfur chemistry is computationally quite challenging. Therefore, the experimental structure of SO₂ was compared with the computational one. The experimentally determined structure^{17,18} yields S–O = 1.434 ± 0.04 Å and <OSO = 119.5 ± 0.3°, while B3LYP/6-31G* yields S–O = 1.464 Å and <OSO = 119.2°, which is just within experimental error. Apart from SO₂, H₂SO₃ plays an important role in the discussion of this article, so the computational results of H₂SO₃ will be examined as well. Once, H₂SO₃ was believed to exist as a rather weak acid in water; however, in the eighties of the former century, evidence was obtained that though almost nonexistent in aqueous solution, it could be obtained via vacuum thermolysis of diethyl sulfite or ethane sulfonic acid¹⁹ thus showing that H₂SO₃(g) intrinsically is (meta) stable and that the environment dictates its stability or instability. B3LYP/6-31G* yields Δ*H*(g) = +2.9 kJ/mol and Δ*G*(g) = +48.2 kJ/mol for the formation of H₂SO₃(g) from H₂O(g) and SO₂(g). The values for H₂SO₃(aq) are Δ*H*(aq) = +3.2 kJ/mol and Δ*G*(aq) = +31.4 kJ/mol, indicating that the formation of H₂SO₃ from H₂O and SO₂ neither in the gas phase nor in the liquid phase will be beyond the trace level, in line with the actual literature. In addition, this article¹⁹ made a HF/6-31G* comparison of two possible isomeric forms of sulfurous acid, (HO)₂SO and H–SO₂(OH), showing an energy difference of 70.2 kJ/mol. B3LYP/6-31G* yields 69.4 kJ/mol. Again, a close match between the B3LYP/6-31G* results and the literature data is observed.

An MMFF structural model for Lewatit R VP OC 1065 is shown in [Figure 1](#) below. The interested reader will find a description and an analysis of all steps leading to this structural model in a former article.⁷

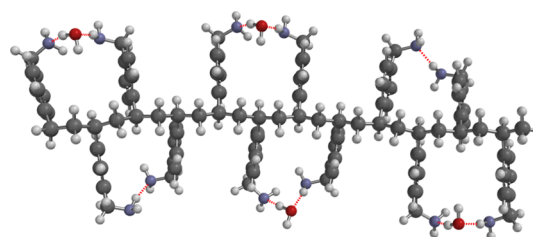


Figure 1. MMFF structural model of Lewatit R VP OC 1065: saturated dodecamer of *p*-vinyl benzyl amine with four pairs of benzyl amino groups each containing a molecule of H₂O. Atoms are displayed as ball and spokes; H: white, C: gray, N: blue, O: red, and H-bridges: red dashed.

In Lewatit R VP OC 1065, benzyl amine groups are orientated perpendicular to the polyvinyl backbone in an alternating mode wherein even and odd benzyl amine groups are within such a close vicinity that they can show H-bridges. Both H-bridging and π -stacking contribute to the stability. Adsorbed H₂O can coordinate to a pair of benzyl amine groups in several modes; however, the one displayed is the most stable. The elemental analysis of the fresh sample of Hallenbeck et al.⁴ corresponds to a structure wherein ~67% of all pairs of benzyl amine groups contains a H₂O molecule. Thus, two types of active sites are present: the first type of active sites shows H-bridging between two alternating benzyl amine groups. The second type is the result of strong physisorption of one molecule of H₂O on a pair of such alternating benzyl amine groups via H-bridging.

For quantum chemical calculations, trimeric units were chosen as they represent the smallest unit still containing the essential structural unit. [Figure 2](#) shows the SO₂ complexes with three trimeric units: a mono amine–SO₂ model, and the two active side models. The mono amine–SO₂ model was chosen to allow structural and energetic comparisons with the two active side models. From a direct comparison between [Figure 1](#) with the dodecameric MMFF structural model and [Figure 2](#) with the trimeric B3LYP/6-31G* models, it can be seen that the basic structural features remain intact for both types of active sites. The dihedral angle between two alternating benzyl amino groups is ~0° for a type 1 complex and ~10° for a type 2 complex as a result of the insertion of an H₂O molecule between the amino groups.

Amine–SO₂ complexes are well known and usually described as charge transfer complexes.^{20–22} The charge transfer is caused by the donation of negative charge from the free electron pair of the amine to SO₂ both to S and the two O atoms. From [Figure 2](#), it can be seen that in the mono amine–SO₂ complex, the two N-atoms of the alternating amino groups show an electrostatic charge of –0.893 and –0.772, while the N-atom of the amino group with SO₂ shows an electrostatic charge of –0.362 only. The S-atom of SO₂ shows an electrostatic charge of 0.512 and its O-atoms show an electrostatic charge of ~–0.364. In free SO₂, the electrostatic charge on S is 0.579 and that on the O-atoms is –0.289. Similar observations can be made in type 1 and 2 active sites, with the lowest electrostatic charge on S of 0.455 on a type 2 active site SO₂ complex.

The solid aniline–SO₂ complex is one of the few primary amine–SO₂ complexes, which are experimentally described in detail,²¹ and therefore, is of interest to compare with the two active site models. Apart from the described electrostatic charge transfer from N to S, it also shows quite strong H-bridging between the H-atoms of the amine and the O-atoms of SO₂, as was concluded from the broad N–H stretching vibration

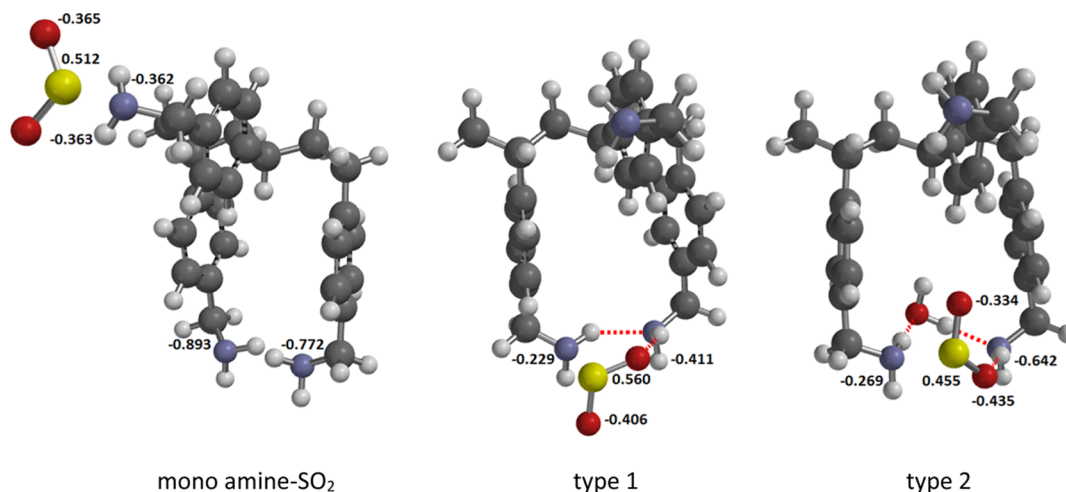


Figure 2. B3LYP/6-31G* type 1 and 2 active site complexes with SO₂ and the corresponding monoamine–SO₂ complex. Atoms are displayed as ball and spokes; H: white, C: gray, N: blue, O: red, S: yellow, and H-bridges: red dashed. Electrostatic charges on N and S were displayed in black.

Table 1. SO₂-Physisorption Energies of the Two Active Site Models for Lewatit R VP OC 1065 and the Trimeric Monoamine–SO₂ Complex

model	ΔH -physisorption (kJ/mol)		$\Delta S_{\text{evap}} \text{-SO}_2$ (J/mol·K) ¹⁷	ΔG (298 K)	ΔG (481 K)
	MMFF	B3LYP/6-31G*		B3LYP/6-31G* (kJ/mol)	B3LYP/6-31G* (kJ/mol)
monoamine–SO ₂	–22.3	–37.6	94.7	–9.4	+8.0
type 1	–53.5	–52.6		–24.3	–7.0
type 2	–60.6	–64.0		–35.8	–18.4

adsorptions (3500–2200 cm^{–1}) and the SO₂ symmetric stretching vibration at 1103 cm^{–1}, which is lower than expected. That SO₂ symmetric stretching vibration is useful to analyze the type 1 and 2 active site–SO₂ complexes too. B3LYP/6-31G* type 1 and 2 active site complexes with SO₂ show a SO₂ symmetric stretching vibration of 1032 cm^{–1} and 1040 cm^{–1}, respectively, while free SO₂ is at 1081 cm^{–1} thus clearly showing H-bridging in both cases in line with the experimental observation on the aniline–SO₂ complex. Next, ΔH of physisorption of SO₂ for the two complexes and a monoamine–SO₂ complex was calculated using both MMFF and B3LYP/6-31G* with respect to the starting complexes and SO₂. In addition, an estimate for ΔG was made, based on ΔH and the experimentally known ΔS_{evap} of SO₂.¹⁷ Table 1 lists the results.

The ΔH -values of MMFF and B3LYP/6-31G* are quite similar for both types of active sites, showing the largest difference (3.6 kJ/mol) for active site type 2, but the values for the monoamine–SO₂ complex deviate strongly. The reason for the deviation is that in the B3LYP/6-31G* structure the SO₂ and NH₂– group are in the same plane (Figure 2) while in the MMFF structure the SO₂ group is orientated perpendicular to the NH₂ group as such a type of H-bridge is not parametrized in MMFF. Similarly the difference for active site type 2 is because of the fact that the B3LYP/6-31G* structure shows a weak electrostatic interaction between an O-atom of SO₂ and a H-atom of H₂O, which again is absent in the MMFF structure.

The ΔH of SO₂ physisorption for the two active site models is very high compared to the monoamine SO₂ complex, once more showing their rather unique character with two amino groups in close vicinity. The ΔH of both complexes is also high compared to that of CO₂ (~–19.5 kJ/mol) and equally high (type 1) or higher (type 2) compared to that of H₂O (–54.9 kJ/mol).⁷ Finally, the ΔH of the three complexes is reflected in their N–S distances with 2.530 cÅ for the monoamine–SO₂ complex,

2.419 Å, for the type 1–SO₂ complex, and 2.306 Å for the type 2–SO₂ complex.

The experimental results of Hallenbeck and Kitchin⁴ contain additional support for the presence of two active sites and they will be discussed below using the computational data of Table 1 and additional calculations.

Competitive Physisorption of SO₂ in the Presence of CO₂. Competitive physisorption of SO₂ (431 ppm) in the presence of 12.5% CO₂ leads to a CO₂ capacity loss of 0.82 mol/kg resin in a virtually linear (zero-order) process in the first 6 cycles (11.8 h). Thereafter, slower SO₂ poisoning eventually leads to an almost complete loss of CO₂ capacity (1.31 mol/kg). The first zero-order SO₂-poisoning process, showing a 0.81/1.31 = 63% CO₂ capacity loss, can be very well explained by SO₂ physisorption on an active site type 2, with a physisorption enthalpy of –64.0 kJ/mol and an average presence of 62% based on the elemental analysis of the starting resin: O = 3.7%. In the next three cycles, the SO₂-poisoning process is almost completed on active site type 1, with a lower physisorption enthalpy of –52.6 kJ/mol.

Thermal Desorption of SO₂. Thermal desorption of SO₂ in a N₂ environment was not successful up to 208 °C. Using the ΔG SO₂-physisorption values of the two active sites listed in Table 1, a K_{eq} value for type 1 of ~6 and a K_{eq} value for type 2 of ~100 at 208 °C (481 K) are obtained in line with the thermal desorption experiments. Explorative calculations, using methyl amine as a very small model, on the possible consecutive formation of CH₃N–SO₂H, and even RN=S=O²⁰ yielded ΔH values of 34.0 and 62.4 kJ/mol, respectively, and a ΔG (481 K) value of +44 kJ/mol for the overall reaction. Thus, consecutive reactions of the amine–SO₂ complexes are very unlikely, even at 208 °C, while the stability of the complexes themselves provide sufficient explanation for all experimental findings.

Chemically Induced Desorption. Chemically induced desorption of the resin was tried by treatment of the resin particles with a solution of 1.5 M NaOH in water. Obviously, the idea behind this is the notion that the SO_2 -complex might undergo transformation into an amine- H_2SO_3 or amine- H^+ - HSO_3^- adduct, which in turn could be converted into a Na^+ HSO_3^- aqueous solution and the free resin.

To get an indication of such a procedure would work with the quite hydrophobic resin, first fresh Lewatit R VP OC 1065 resin was treated with 1.5 M H_2SO_4 in water followed by rinsing with water to remove excess sulfuric acid. Next, the sulfated resin was treated with 1.5 M NaOH in water for 3 days, and thereafter, its CO_2 capacity was measured. Complete recovery of CO_2 capacity was observed showing that the procedure with respect to acid-base reaction rate and transport to the aqueous phase was adequate. Furthermore, elemental analysis showed complete removal of S as sulfate, while the remaining amount of O (3.1%) as H_2O is consistent with 50% of type 2 active sites.

Applying the same procedure to the SO_2 -poisoned resin yielded a recovery of $0.48/1.31 = 37\%$ CO_2 capacity only. Elemental analysis of the SO_2 -poisoned resin treated with the NaOH solution still yielded the presence of SO_2 rather than sulfite species, assuming that in this case also 3.1% of O is present as H_2O in type 2 active sites (50%). Therefore, the stability and formation of amine- H_2SO_3 adducts from the two types of active sites was computationally investigated. Figure 3 shows the adducts of H_2SO_3 with the amine groups of the two types of active sites.

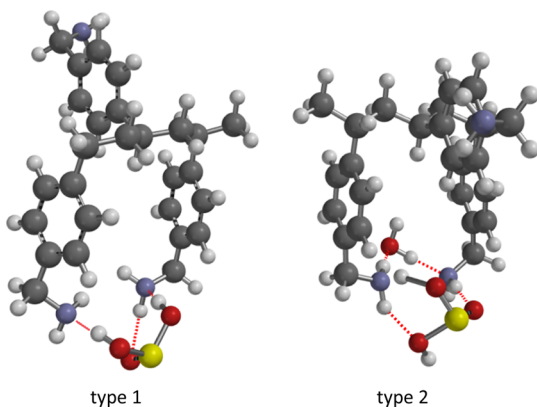


Figure 3. B3LYP/6-31G* type 1 and 2 active site adducts with H_2SO_3 . Atoms are displayed as ball and spokes; H: white, C: gray, N: blue, O: red, S: yellow, and H-bridges: red dashed.

Geometry optimization of a type 1 active site with H_2SO_3 leads to an amine- H_2SO_3 adduct wherein the two OH groups of H_2SO_3 form H-bridges to the two amine groups: the $\text{OH}\cdots\text{N}$ distances are 1.716 and 1.731 Å, respectively. The H-bridge between the two amine groups present both in the type 1 active site and the corresponding type 1 active site- SO_2 complex has disappeared. Direct formation of H_2SO_3 from a type 2 active site might lead to a type 1 active site amine- H_2SO_3 adduct too.

Geometry optimization of a type 2 active site with H_2SO_3 leads to an amine- H^+ - HSO_3^- adduct wherein two $\text{NH}\cdots\text{O}$ hydrogen bridges are present with distances of 1.977 and 1.931 Å, respectively. One H-atom of H_2SO_3 has been transferred to an amine group with a N-H distance of 1.061 Å and an SO-H distance of 1.662 Å, thus creating an $\text{NH}\cdots\text{OS}$ H-bridge. The H-bridges between the amine groups and H_2O remain intact as in

type 2 active site and its SO_2 -complex. It is remarkable that the presence of one extra H_2O molecule as present in a type 2 active site compared to a type 1 active site shifts the nature of the adduct from an amine- H_2SO_3 adduct to an amine- H^+ - HSO_3^- adduct. The transition states for both reactions were determined, as shown in Figure 4.

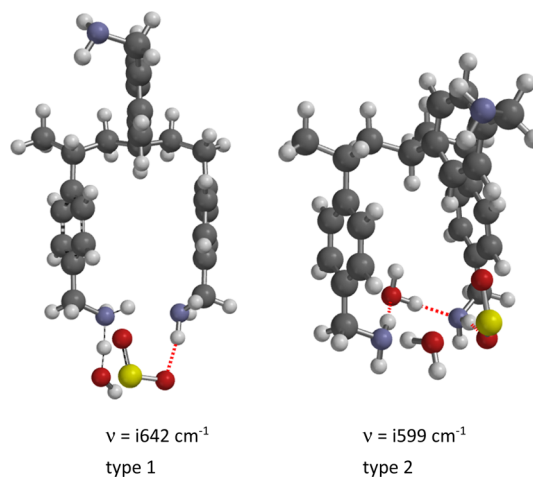


Figure 4. B3LYP/6-31G* transition states for type 1 and 2 active site- H_2SO_3 adducts. Atoms are displayed as ball and spokes; H: white, C: gray, N: blue, O: red, S: yellow, and H-bridges: red dashed.

The process in both cases is very similar: the unique imaginary frequencies show simultaneous movement of H^+ from H_2O to an amine group and H_2O - SO_2 covalent bond formation. The distances are: $\text{N}\cdots\text{HOH} = 1.274$ Å and 1.283 Å, and $\text{H}_2\text{O}\cdots\text{SO}_2 = 2.108$ Å and 2.131 Å for type 1 and 2 active site transition states. However, the outcome is different with an amine- H_2SO_3 adduct for a type 1 active site and an amine- H^+ - HSO_3^- adduct for a type 2 active site. The activation barriers are 12.8 and 24.4 kJ/mol for type 1 and type 2 active site, respectively, thus no kinetic limitation is expected.

Both processes are equilibrium reactions with ΔH of +5.4 kJ/mol and $K_{\text{eq}}(298 \text{ K}) = 0.11$, and -2.5 kJ/mol and $K_{\text{eq}}(298 \text{ K}) = 2.7$ for type 1 and type 2 active sites, respectively. ΔH values were calculated starting from complexes with an additional H_2O molecule underneath the SO_2 complexes to mimic the presence of additional H_2O in the liquid phase as in the experimental chemical desorption procedure. ΔH of direct formation of an amine- H_2SO_3 adduct from a type 2 active site SO_2 complex is slightly more endothermic with +12.0 kJ/mol and $K_{\text{eq}}(298 \text{ K}) = 7.9 \times 10^{-3}$. With the computational values obtained, a total recovery of 5% (type 1 active site) + 37% (type 2 active site) = 42% CO_2 capacity is obtained close to the experimental value of 37%. As described above, Hallenbeck and Kitchin⁴ used aqueous NaOH to remove SO_2 adsorbed on the resin. OH^- is certainly able to deprotonate amine- H^+ ; however, Na^+ does not have a good affinity for the HSO_3^- anion. Tudela and Jenkins²³ showed that Rb^+ and Cs^+ stabilize HSO_3^- much better in the solid phase by -40 and -59 kJ/mol, respectively, compared to $\text{NaHSO}_3(\text{s})$. The conductor-like polarizable continuum model (C-PCM)²⁴ was applied in combination with B3LYP/6-31G* using the equation

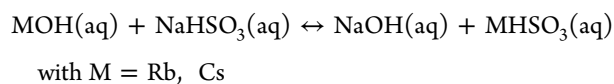


Table 2. Selected Physical Properties of PD-APS and PD-MAPS¹⁰

material	amine loading (mmol N/g)	S_{BET} (m ² /g)	$S_{\text{propylamine}}^b$ (πr^2 in cS ²)	$N/S_{\text{propylamine}}$	CO ₂ capacity ^a (mmol/g)	SO ₂ capacity ^a (mmol/g)
PD-APS-1	1.3	227	46.3	1.6		
PD-APS-2	1.9	213		2.5	0.72	0.70
PD-APS-4	3.7	57		18.1		
PD-MAPS-1	1.3	255		1.4		
PD-MAPS-2	2.1	150		3.9	0.75	1.08
PD-DMAPS-2	1.9	111		4.8		

^aAt 200 ppm of SO₂. ^bThe distance C₃–N = 3.840 Å in propyl amine was taken as r .

Table 3. ΔH CO₂, ΔH SO₂, $\Delta G(383 \text{ K})$ CO₂, and $\Delta G(383 \text{ K})$ SO₂ Computational Values (B3LYP/6-31G*); ΔS_{evap} CO₂ and ΔS_{evap} SO₂ Are Derived from the NIST Chemistry Webbook¹⁷

material	model	ΔH CO ₂ (kJ/mol)	ΔH SO ₂ (kJ/mol)	$\Delta G(383 \text{ K})$ CO ₂ (kJ/mol)	$\Delta G(383 \text{ K})$ SO ₂ (kJ/mol)
PD-APS	propyl amine	−17.5	−40.3	15.8	−4.0
	(propyl amine) ₂	−21.9	−65.0	11.4	−28.7
PD-MAPS	<i>N</i> -methyl propyl amine	−15.9	−45.0	17.4	−8.7
	(<i>N</i> -methyl propyl amine) ₂	−21.2	−69.5	12.1	−33.2
PD-DMAPS	<i>N,N</i> -dimethyl propyl amine	−14.2	−44.4	19.1	−8.1

RbHSO₃(aq) and CsHSO₃(aq) turn out to be −48.0 and −59.3 kJ/mol, respectively, more stable than NaHSO₃(aq) in line with the results of Tudela and Jenkins.²³ The results suggest that the use of aqueous RbOH or CsOH might lead to complete regeneration of the resin; however, the remaining aqueous metal sulfite solution requires a number of additional steps to obtain a useable SO₂ stream, and thus, does not look economically viable.

As mentioned in the introduction, Rezaei and Jones^{10,11} reported SO₂ deactivation on aminosilica absorbents for CO₂ capture using primary, secondary, and tertiary amine starting materials with various loadings. Here, only a part of their work will be discussed, which is relevant for the comparison with Lewatit R VP OC 1065. PD09024 from PQ Corporation was functionalized through the reaction of 3-aminopropyl trimethoxysilane (APS), *N*-methyl 3-aminopropyl trimethoxysilane (MAPS) or *N,N*-dimethyl 3-aminopropyl trimethoxysilane (DMAPS) with surface silanols to yield the corresponding aminosilica materials PD-APS, PD-MAPS, and PD-DMAPS.

It was observed¹⁰ that both PD-APS and PD-MAPS show an almost linear increase of SO₂ capture and an almost linear decrease in normalized CO₂ capture with SO₂ concentration (20–200 ppm). For these CO₂ capture experiments, the SO₂-exposed materials first underwent a regeneration procedure at 110 °C with helium. PD-DMAPS shows by far the lowest SO₂ capture and no CO₂ capture under the experimental conditions (dry inert gas). The effect of amine loading of the material was also investigated. It was found that PD-APS, PD-MAPS, and PD-MAPS show an almost linear increase of SO₂ capture with amine loading but the increase for PD-DMAPS is quite small. At the same time, the so called amine efficiency, expressed as mmol amine/mmol SO₂, increases from ~0.24 at 1.6 mmol N/g via 0.27 at 2.3 mmol N/g to 0.31 at 3.7 mmol N/g for DP-APS, and 0.24 at 1.6 mmol N/g to 0.51 at 2.1 mmol N/g for PD-MAPS. Again, the effect for PD-DMAPS is small: an increase from 0.09 at 1.3 mmol N/g to 0.12 at 1.9 mmol N/g. In their second study, Rezaei and Jones¹¹ performed SO₂/CO₂ coadsorption experiments at various SO₂ levels (20, 200 ppm) and 10% CO₂. It was observed that the SO₂ breakthrough curves at 200 ppm of SO₂ follow the order PD-DMAPS, PD-APS, and PD-MAPS. Next, two types of coadsorption cycles were executed: (1) with CO₂ breakthrough, and (2) with SO₂ breakthrough as a decisive point in the cycle. In both cases, there is an initial loss of the

normalized CO₂ capacity after which a kind of plateau is reached. The decrease is larger for the SO₂ breakthrough than for the CO₂ breakthrough experiments. No large difference in behavior between PD-APS and PD-MAPS was observed. The initial loss of CO₂ capacity was explained as irreversible SO₂ adsorption on some amine sites to a certain level next to reversible SO₂ adsorption on other amine sites.

In order to allow a meaningful comparison between Lewatit R VP OC 1065 and the aminosilica absorbents, a computational approach was chosen based on experimental results discussed above and the physical properties of these materials, which are summarized in Table 2. Amine loading, S_{BET} , remaining CO₂ capacity, and SO₂ capacity after exposure to 200 ppm of SO₂ were taken from Rezaei and Jones.¹⁰ $S_{\text{propylamine}}$ is the surface of a circle with $r = 3.840 \text{ \AA}$ as the distance C₃–N in propyl amine. As described by the authors, it is assumed that reaction of an APS leads to a Si–C bond pointing out of the silica surface, leaving the C₃–N distance as the radius of a circle that can be reached by the amino group. Next, $N/S_{\text{propylamine}}$ is calculated by dividing the number of amine sites by the S_{BET} and multiplying with $S_{\text{propylamine}}$. This number shows how many amine groups, depending on their conformation, can be in close vicinity of each other. This property is of great importance to allow a comparison with Lewatit R VP OC 1065, which shows inherently dimeric amine groups as type 1 and type 2 active sites.

From Table 2 column $N/S_{\text{propylamine}}$, it is clear that for all materials already from the lowest amine loading, at least a fraction of the amine groups can be within close vicinity of each other, and that that fraction will increase with its amine loading. Therefore, in the computational approach, two options were investigated for each model of CO₂ and SO₂ active sites of the materials: a monomeric one and a dimeric one. In Lewatit R VP OC 1065, only dimeric active sites are present. For PD-DMAPS, only a monomeric active site was considered, as in the absence of H-atoms on the amine, stable dimers are unlikely. Table 3 shows the computational results for the various models.

From Table 3, it becomes clear that CO₂ capture by PD-APS and PD-MAPS cannot be explained by physisorption neither on monomeric nor dimeric sites. Thus, the only remaining explanation for CO₂ capture is chemisorption. The product of that chemisorption can only be a carbamic acid under the dry experimental conditions, and this requires dimeric sites to allow

amine catalysis as described for Lewatit R VP OC 1065⁷. As discussed above, dimeric sites are likely for all materials except for PD-DMAPS, and indeed PD-DMAPS shows no CO₂ capture. With respect to SO₂ capture or deactivation, it can be seen that both monomeric and dimeric active sites are capable of capturing SO₂ wherein monomeric sites show reversible SO₂ capture and dimeric sites show irreversible SO₂ capture. Even the experimental differences between PD-APS, PD-MAPS, and PD-DMAPS are reflected satisfactory. Thus, the computational approach and results based on the analysis of the experimental results as listed in Table 2 offer a consistent explanation for the CO₂ capture and SO₂ deactivation behavior of these materials. In fact, the behavior of the dimeric sites of the aminosilica sorbents is very similar to the inherent dimeric active sites of Lewatit R VP OC 1065.

It can be concluded that the mechanism for irreversible SO₂ deactivation of Lewatit R VP OC 1065 is the barrier-free formation of very strong charge transfer complexes of SO₂ with the dimeric active amine sites. The behavior of Lewatit R VP OC 1065 toward SO₂ is paralleled in the partly irreversible deactivation of the aminosilica sorbents PD-APS and PD-MAPS. As deactivation by SO₂ of Lewatit R VP OC 1065 is largely irreversible, it becomes opportune to develop a procedure to avoid SO₂ deactivation, which will be discussed below.

Procedure To Avoid SO₂ Deactivation of Lewatit R VP OC 1065. Procedures to avoid SO₂ deactivation of Lewatit R VP OC 1065 in CO₂-capturing processes can be divided into two basic scenarios: (a) SO₂ poisoning of Lewatit R VP OC 1065 in Direct Air Capture of CO₂, and (b) SO₂ poisoning of Lewatit R VP OC 1065 in CO₂ capture from flue gas from either coal burning or fuel oil burning.

(a) SO₂ poisoning of the resin in Direct Air Capture of CO₂

In the introduction, it was mentioned that nowadays the average level of SO₂ in the atmosphere has gone down to ~20 ppb, which would not require additional measures to avoid SO₂ poisoning of the resin. However, occasionally a peak level of 700 ppb of SO₂ can be observed, which could easily deactivate the resin within one year. Nowadays, air pollution, including SO₂, is globally monitored²⁵ and with TROPOMI very high-resolution local maps can be obtained too. Such data can be used to temporarily halt the operation of a Direct Air Capture of CO₂ installation. Even if this would count up to one day/month, it will be by far the cheapest measure to avoid SO₂ deactivation of the resin.

(b) SO₂ poisoning of the resin in CO₂ capture from flue gas from either coal or fuel oil burning.

As described in the Introduction, both coal-fired power plants and fuel oil using large ships are nowadays still important sources of CO₂ and SO₂ emission. CO₂ and SO₂ capture from both sources will contribute to lower the carbon foot print and further improvement of the air quality. It looks much better to focus on SO₂ itself as a primary product as large amounts of SO₂ are oxidized to sulfuric acid, furthermore, it is used in the food and beverage industry as an antioxidant, and finally it is used as a feedstock for various chemicals.

In the literature,^{26–29} several PEG-based materials are mentioned, which could capture SO₂ and showing at the same time good separation factors for SO₂/CO₂. Already in 1995, Chakma²⁶ reported a liquid membrane system consisting of an immobilized PEG (PEG 400) liquid membrane in series with another immobilized diethanol amine (DEA)/PEG 400

membrane. PEG 400 preferentially adsorbs SO₂ while the CO₂ was caught by the DEA containing membrane. In the PEG 400 membrane, an average separation factor SO₂/CO₂ = 13 was measured independent of the SO₂ pressure differential over the liquid membrane.

In 2012, Yang et al.²⁷ reported on a system built up from the nonfunctionalized trimer of ethylene glycol (PEG 150) as a solvent combined with a PEG-functionalized basic ionic liquid (IL) derived from diazobicyclooctane (DABCO). The PEG 150/PEG 150 MeDABCO bis(trifluoromethylsulfonyl)imide (NTf₂) system showed a SO₂ capacity of 4.38 mol/mol IL at a 0.1 bar SO₂ partial pressure. In 2013, Yang et al.²⁸ reported on another comparable system built up from PEG-150 combined with an imidazole functionalized trimer of ethylene glycol (PEG 150/MeIm PEG 150). At 1.0 bar of SO₂, PEG 150 showed a SO₂ capacity of 1.32 mol SO₂/mol PEG while the MeIm PEG 150/PEG 150 = 1/1 mixture showed a SO₂ capacity of 4.88 mol SO₂/mol MeIm PEG 150/PEG 150 mixture. The larger SO₂ uptake of the MeIm PEG 150/PEG 150 mixture was contributed to the formation of a sulfite catalyzed by the imidazole-functionalized trimer of ethylene glycol. The use of *N*-octyl imidazole as a nonvolatile catalyst leads to a very similar result. Their ratio SO₂/CO₂ = 26.5 was obtained from the separate capacities of both materials for SO₂ and CO₂.

In 2016, Zhao et al.²⁹ reported an SO₂ uptake of 7.32 mmol SO₂/kg PEG 600 at 500 ppm SO₂. However, the system is sensitive to the amount of H₂O, showing a gradual decrease from 7.32 mmol/kg 100% PEG 600 + 0% H₂O to a minimum level of 1.65 mmol SO₂/kg 60% PEG 600 + 40% H₂O, followed by a gradual increase to 3.29 mmol SO₂/kg in pure water (0% PEG 600 + 100% H₂O). For each mass fraction of PEG 600, its SO₂ solubility could be adequately described by Henry's law. FT-IR provided further evidence that SO₂ as such was adsorbed.

Some explorative computational work was performed to understand the experimental findings cited above. PEG 150, corresponding to a linear trimer of ethylene glycol, was used as a structural model for comparative computational work. A conformer distribution of the trimer yielded a series of conformers wherein the two OH-end groups form a hydrogen bridge with the ether-O in the β-position of the chain. These internal hydrogen bridges are maintained to conformer 6, yielding 74% in the cumulative Boltzmann weights. Now, this is a gas-phase situation, so it is expected that in the liquid-phase, hydrogen bridging will take place not only intramolecularly but also intermolecularly. Figure 5 shows the two principal types of

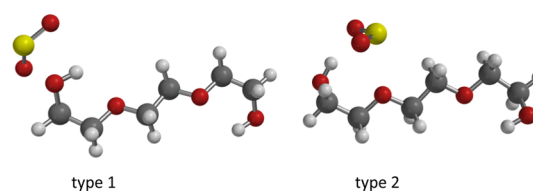


Figure 5. B3LYP/6-31G* type 1 and 2 complexes of the trimer of ethylene glycol with SO₂. Atoms are displayed as ball and spikes; H: white, C: gray, O: red, and S: yellow.

SO₂ complexes using the best conformer of the trimer ethylene glycol. Type 1 shows complexation of SO₂ to the alcohol of the trimer of ethylene glycol (S...OH = 2.607 Å) and a weak SO...HO H-bridge (SO...HO = 2.812 Å). Type 2 shows complexation of SO₂ to the ether of the trimer of ethylene glycol (S...OR₂ = 2.861 Å) and a SO...HO H-bridge (SO...HO = 2.069 Å).

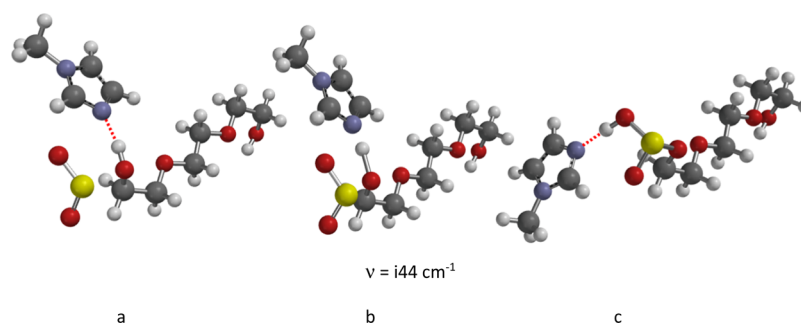


Figure 6. B3LYP/6-31G* starting complex (a), transition state (b), and primary postreaction complex (c) of the N-Me imidazole-catalyzed formation of the sulfurous acid monoester of the trimer of ethylene glycol with SO₂. Atoms are displayed as ball and spokes; H: white, C: gray, N: blue, O: red, S: yellow, and H-bridges: red dashed.

In type 1, the OH...OR₂ H-bridges, present in the best conformer of the trimer of ethylene glycol, remain intact (OH...OR₂ = ~2.25 Å). In type 2, only one OH...OR₂ H-bridge remains intact (OH...OR₂ = 2.318 Å). $\Delta H(298)$ s of both processes are -28.4 kJ/mol and -18.0 kJ/mol for type 1 and 2, respectively. Thus, complexation of SO₂ to an alcohol function is more favorable than to an ether function, though with increasing chain length of the PEG, the number of ether functions does increase as SO₂ complexation on complex type 2 will do also as observed by Yang et al.^{27,28} Using the experimentally known ΔS_{evap} of SO₂,¹⁷ $\Delta G(298 \text{ K})$ for type 1 = -0.2 kJ/mol results, corresponding to $K_{\text{eq}}(298 \text{ K})$ s = 1.09 in line with the easy desorption of SO₂ at 298 K under N₂.²⁷⁻²⁹ Complexation of CO₂ to the trimer of ethylene glycol yields a ΔH = -14.3 and -11.0 kJ/mol for type 1 and type 2, respectively, and thus, confirms the high experimentally observed selectivity of SO₂ over CO₂.

The PEG 150/PEG 150 MeDABCO NTf₂ and the PEG 150/MeIm PEG 150 system, are different. Here, adsorption of SO₂ starts with the formation of a PEG 150 MeDABCO NTf₂ or a MeIm PEG 150 SO₂ charge transfer complex as described earlier for Lewatit R VP OC 1065 and the aminosilica adsorbents. ΔH s of the N-Me⁺ DABCO Br⁻—and N-Me imidazole—SO₂ complexes are -32.5 and -35.9 kJ/mol, respectively, considerably weaker than the PD-DMAPS—SO₂ complex (-44.4 kJ/mol) listed in Table 3. However, in time, the SO₂ complexes react with the alcohol functions of PEG 150 to yield PEG-sulfites. The DABCO or imidazole tertiary amine base acts as a catalyst. The formation of a sulfite catalyzed by tertiary amine base was computationally investigated too, using N-Me imidazole and N-Me⁺ DABCO Br⁻ as catalyst models.

Figure 6 shows the starting complex, the transition state, and the primary postreaction complex with N-Me imidazole as a catalyst model. The activation barrier of the N-Me imidazole catalyzed reaction is 30.8 kJ/mol. The animation of the very low unique imaginary frequency of $\nu = i44 \text{ cm}^{-1}$ shows the simultaneous proton transfer of the alcohol to N-Me imidazole and the formation of a covalent bond between SO₂ and the alcohol. However, according to the B3LYP/6-31G* calculation, the primary reaction product is not an imidazolium sulfite monoester but an imidazole...sulfurous acid monoester adduct showing an N...HOSO₂R H-bridge with a length of 1.696 Å. The final product is the sulfurous acid monoester of the trimer of ethylene glycol with an SOH...O-ether H-bridge with a length of 1.789 Å. Using N-Me DABCO Br as a catalyst model, an activation barrier of 43.6 kJ/mol was obtained in a very similar process. ΔH of the reaction is +0.3 kJ/mol, which leads to a $K_{\text{eq}}(298 \text{ K}) = 0.89$, typical for an equilibrium reaction. Thus,

combined physisorption and chemisorption leads to a large amount of SO₂ captured, which can also easily be released in line with the experimental observations of Yang et al.^{27,28}

All these properties make the application of a PEG system with an N-alkyl imidazole derivative or PEG 150 MeDABCO NTf₂ very promising for SO₂ capture prior to CO₂ capture by Lewatit R VP OC 1065. Capturing both gases is an environmentally very attractive option for flue gas originating from coal-fired power plants and fuel oil for large ships. The only remaining critical point might be the sensitivity for H₂O uptake,²⁹ not only with respect to SO₂ capacity but also for the overall energy consumption of the process. Flue gas will contain a lot of H₂O and this should not adsorb in the PEG system.

CONCLUSIONS

- SO₂ deactivation of Lewatit R VP OC 1065 is caused by the irreversible formation of two dimeric amine—SO₂ charge transfer complexes, which are very stable, and cannot be regenerated to the starting dimeric amine complexes by thermal desorption up to 208 °C. Under the various process conditions for CO₂ capture, further reaction with amine—H₂SO₃ adducts is unlikely as the thermodynamics are unfavorable.
- Chemical desorption using 1.5 M NaOH in water was only partly successful with a recovery of 37% of the CO₂ uptake capacity. Computational analysis of this experimental work supports these findings but the use of aqueous RbOH or CsOH instead of NaOH might lead to complete regeneration of the resin. However, it is unlikely that this procedure could be developed into a commercially viable process.
- In Direct Air Capture of CO₂ using Lewatit R VP OC 1065, SO₂ deactivation is best avoided by temporary halting operation if a peak level of SO₂ is expected. Under normal conditions, the atmospheric level is sufficiently low to be harmless for the resin.
- PEG/N-alkyl imidazole and PEG/DABCO-PEG systems show a high selectivity of SO₂ over CO₂, a good uptake of SO₂, and are easily regenerated to the starting systems and a concentrated SO₂ stream at room temperature. The amine bases have two functions: (a) they act as initial catchers of SO₂ by the formation of moderately strong tertiary amine—SO₂ charge transfer complexes, and (b) they act as catalysts to convert SO₂ and the PEG-alcohol functions into sulfites in an overall equilibrium reaction.
- A combination of a PEG/DABCO-PEG or N-alkyl imidazole system with Lewatit R VP OC 1065 is an

environmentally very promising process option to capture both SO₂ and CO₂ from flue gas, originating from coal-fired power plants and large ships.

- Molecular modeling work in this study quantitatively supports and explains the experimental findings of experimental work on Lewatit RVP OC 1065, aminosilica materials, and various PEG systems.

■ ASSOCIATED CONTENT

Supporting Information

The Supporting Information is available free of charge at <https://pubs.acs.org/doi/10.1021/acs.iecr.0c01800>.

Description of Supporting Information files (PDF)

Molecular modelling data (XLSX)

All molecular structures [task name_method.pdb] (ZIP)

■ AUTHOR INFORMATION

Corresponding Author

Wim Buijs – Process & Energy Department, Faculty of Mechanical, Maritime and Materials Engineering, Delft University of Technology, 2628 CB Delft, The Netherlands;
orcid.org/0000-0003-3273-5063; Email: w.buijs@tudelft.nl

Complete contact information is available at:
<https://pubs.acs.org/doi/10.1021/acs.iecr.0c01800>

Notes

The author declares no competing financial interest.

■ REFERENCES

- IPCC. *IPCC Special Report on Carbon Dioxide Capture and Storage. Prepared by Working Group III of the Intergovernmental Panel on Climate Change*; Metz, B., Davidson, O., de Coninck, H. C., Loos, M., Meyer, L. A., Eds.; Cambridge University Press: Cambridge, United Kingdom, 2005; p 442.
- IEA. *CO₂ Emissions from Fuel Combustion 2018*, IEA, Paris (2018), (accessed February 2020).
- Alesi, W. R., Jr.; Kitchin, J. R. Evaluation of a Primary Amine-Functionalized Ion-Exchange Resin for CO₂ Capture. *Ind. Eng. Chem. Res.* **2012**, *51*, 6907–6915.
- Hallenbeck, A. P.; Kitchin, J. R. Effects of O₂ and SO₂ on the Capture Capacity of a Primary-Amine Based Polymeric CO₂ Sorbent. *Ind. Eng. Chem. Res.* **2013**, *52*, 10788–10794.
- Hallenbeck, A. P. Micro-scale Approaches to the Bench-Scale Evaluation of CO₂ Capture System Properties. PhD Thesis, Carnegie Mellon University, Pittsburgh, April 19, 2016.
- Yu, Q.; Delgado, J. d. I. P.; Veneman, R.; Brilman, D. W. F.; Brilman, D. W. F. Stability of a Benzyl Amine Based CO₂ Capture Adsorbent in View of Regeneration Strategies. *Ind. Eng. Chem. Res.* **2017**, *56*, 3259–3269.
- Buijs, W.; de Flart, S. Direct Air Capture of CO₂ with an Amine Resin: A Molecular Modeling Study of the CO₂ Capturing Process. *Ind. Eng. Chem. Res.* **2017**, *56*, 12297–12304.
- Buijs, W. Direct Air Capture of CO₂ with an Amine Resin: A Molecular Modeling Study of the Deactivation Mechanism by CO₂. *Ind. Eng. Chem. Res.* **2019**, *58*, 14705–14708.
- Buijs, W. Direct Air Capture of CO₂ with an Amine Resin: A Molecular Modeling Study of the Oxidative Deactivation Mechanism with O₂. *Ind. Eng. Chem. Res.* **2019**, *58*, 17760–17767.
- Rezaei, F.; Jones, C. W. Stability of Supported Amine Adsorbents to SO₂ and NO_x in Postcombustion CO₂ Capture. 1. Single-Component Adsorption. *Ind. Eng. Chem. Res.* **2013**, *52*, 12192–12201.
- Rezaei, F.; Jones, C. W. Stability of Supported Amine Adsorbents to SO₂ and NO_x in Postcombustion CO₂ Capture. 2. Multicomponent Adsorption. *Ind. Eng. Chem. Res.* **2014**, *53*, 12103–12110.
- <https://www.epa.gov/air-trends/sulfur-dioxide-trends> (accessed April 2020).
- https://www.developmentaid.org/api/frontend/cms/uploadedImages/2019/10/Air-quality-in-europe_2019-final.pdf (accessed and downloaded April 2020).
- <http://www.air-quality.org.uk/04.php> (accessed April 2020).
- ExxonMobil: What Does IMO's 0.50% Sulphur Cap Decision Mean for the Bunker Supply Chain? <https://www.exxonmobil.com/en/marine/technicalresource/news-resources/imo-sulphur-cap-and-mgo-hfo> (accessed February 2020).
- Spartan*; Wavefunction Inc.: 18401 Von In Karman Avenue, Suite 370, Irvine, CA 92612 U.S.A., 1994, www.wavefun.com.
- National Institute of Standards and Technology (NIST). <https://www.nist.gov/>; SO₂: <https://webbook.nist.gov/cgi/inchi/InChI%3D1S/O2S/c1-3-2>; CO₂: <https://webbook.nist.gov/cgi/inchi?ID=C124389&Mask=4> (accessed June 2020).
- Holder, C. H., Jr.; Fink, M. Structure determination of SO₂ by electron diffraction. *J. Chem. Phys.* **1981**, *75*, 5323.
- Sülzle, D.; Verhoeven, M.; Terlouw, J. K.; Schwarz, H. Generation and Characterization of Sulfurous Acid (H₂SO₃) and of Its Radical Cation as Stable Species in the Gas Phase. *Angew. Chem., Int. Ed. Engl.* **1988**, *27*, 1533–1534.
- Hata, T.; Kinumaki, S. Reactions of Ammonia and Aliphatic Amines with Sulphur Dioxide. *Nature* **1964**, *203*, 1378–1379.
- Faria, D. L. A.; Santos, P. S. Raman and Infrared Spectra of Some Aromatic Amine-Sulphur Dioxide Molecular Complexes. *J. Raman Spectrosc.* **1988**, *19*, 471–478.
- Emmett, E. J.; Willis, M. C. The Development and Application of Sulfur Dioxide Surrogates in Synthetic Organic Chemistry. *Asian J. Org. Chem.* **2015**, *4*, 602–611.
- Tudela, D.; Jenkins, H. D. B. New Methods To Estimate Lattice Energies: Application to the Relative Stabilities of Bisulfite (HSO₃⁻) and Metabisulfite (S₂O₅²⁻) Salts. *J. Chem. Educ.* **2003**, *80*, 1482.
- Tomasi, J.; Mennucci, B.; Cammi, R. Quantum mechanical continuum solvation models. *Chem. Rev.* **2005**, *105*, 2999–3094.
- Global Sulfur Dioxide Monitoring. Home Page: <https://so2.gsfc.nasa.gov/> (accessed April 2020).
- Chakma, A. Separation of CO₂ and SO₂ from flue gas streams by liquid membranes. *Energy Convers. Mgmt* **1995**, *36*, 405–410.
- Yang, Z.-Z.; He, L.-N.; Song, Q.-W.; Chen, K.-H.; Liu, A.-H.; Liu, X.-M. Highly efficient SO₂ absorption/activation and subsequent utilization by polyethylene glycol-functionalized Lewis basic ionic liquids. *Phys. Chem. Chem. Phys.* **2012**, *14*, 15832–15839.
- Yang, Z.-Z.; He, L.-N.; Zhao, Y.-N.; Yu, B. Highly Efficient SO₂ Absorption and Its Subsequent Utilization by Weak Base/Polyethylene Glycol Binary System. *Environ. Sci. Technol.* **2013**, *47*, 1598–1605.
- Zhao, T.; Qiao, X.; Xu, Q.; Xie, X.; Wei, X.; Zhang, J. Solubility and Spectral Investigation of Dilute SO₂ in the Binary System Polyethylene Glycol 600 + Water and System's Density, Viscosity, and Surface Tension. *J. Mol. Liq.* **2016**, *223*, 224–234.